Bioactive Materials 5 (2020) 1102–1112

Contents lists available at ScienceDirect

Bioactive Materials

journal homepage: http://www.keaipublishing.com/biomat

A pretargeting nanoplatform for imaging and enhancing anti-inflammatory drug delivery

Min Kyung Khang[a,b], Jun Zhou[b], Cynthia M. Co[b], Shuxin Li[b], Liping Tang[b,*]

[a] Department of Chemistry and Biochemistry, University of Texas at Arlington, 700 Planetarium Place, Chemistry Physics Building Room 130, Arlington, TX, 76019-0065, USA

[b] Department of Bioengineering, University of Texas at Arlington, Engineering Research Building, Room 226, Box 19138, Arlington, TX, 76010, USA

ARTICLE INFO

Keywords:
Polymeric micelles
Neutravidin/biotin system
Pretargeting
Macrophages
Dexamethasone
Inflammatory responses

ABSTRACT

This work details a newly developed "sandwich" nanoplatform via neutravidin-biotin system for the detection and treatment of inflammation. First, biotinylated- and folate-conjugated optical imaging micelles targeted activated macrophages via folate/folate receptor interactions. Second, multivalent neutravidin proteins in an optimal concentration accumulated on the biotinylated macrophages. Finally, biotinylated anti-inflammatory drug-loaded micelles delivered drugs effectively at the inflammatory sites via a highly specific neutravidin-biotin affinity. Both *in vitro* and *in vivo* studies have shown that the "sandwich" pretargeting platform was able to diagnose inflammation by targeting activated macrophages as well as improve the therapeutic efficacy by amplifying the drug delivery to the inflamed tissue. The overall results support that our new pretargeting platform has the potential for inflammatory disease diagnosis and treatment.

1. Introduction

The development of drug delivery platforms have been accelerated based on the idea of combining both of the targeting ligands and the imaging/therapeutic agents into a single platform [1–4]. While some advancements have been made thus far in the area of cancer diagnosis and treatment [2,3,5], little progress has been made in developing theranostic platforms for inflammatory diseases which was the goal of this investigation.

A number of pretargeting systems for theranostic cancer treatment have been reported in the literature so far [6–9]. Two-step processes were broadly employed in those systems. Briefly, the first step was to direct the accumulation of an imaging/pretargeting agent at the disease site. Then, the second step was to deliver the therapeutic agent to the diseased tissue by interacting with the pretargeting agent [10–12]. For instance, radiolabeled monoclonal antibodies (mAbs) and radio-immunoconjugates had been combined and reported as a pretargeting platform for cancer diagnosis and treatment [7,13]. Those reports have shown that the pretargeting strategy with a radio-immunodetection (RID) agent and radio-immunotherapeutic (RIT) agent had a much higher tumor specificity (tumor/non-tumor (T/NT) ratio) than the conventional approach. The benefits of this pretargeting strategy include minimal exposure of normal tissues to therapeutic agents and less hematological toxicity [14]. Although those efficient benefits have been applied on tumor detection/treatment, such an approach has not been investigated for theranostic inflammatory disease treatment.

Non-covalent affinity interactions are the most common pretargeting strategy [15,16]. Amongst non-covalent binding systems, avidin/biotin system has been widely studied because it is one of the strongest non-covalent bonds (dissociation constant:10^{-15} M), with the avidin protein having multiple binding sites of biotin [15,17]. In fact, the avidin/biotin system has been extensively utilized in a biochemical assay and affinity purification due to its unique advantages including signal amplification, high specificity and robust stability [18]. However, the avidin/biotin system has limited *in vivo* applications due to the following deficiencies. First, avidin may cross-react with endogenous biotin or lectin. Second, biotinylated molecule can bind to endogenous biotin-binding proteins such as eggs or bacteria [19]. To overcome these limitations, an avidin analogue, streptavidin, derived from *Streptomyces avidinii*, has been exploited as a pretargeting platform. The streptavidin/biotin system has an excellent binding affinity with significantly low non-specific binding [20,21]. However it also has limited utility *in vivo* due to streptavidin's high affinity to fibronectin and kidney tissue [22,23]. In recent years, neutravidin is emerging as an

Abbreviations: BMC, biotinylated micelle; BFMC, biotinylated- and folate-conjugated micelle; FMC, folate-conjugated micelle; Dex, Dexamethasone

Peer review under responsibility of KeAi Communications Co., Ltd.

* Corresponding author. Department of Bioengineering, University of Texas at Arlington, P.O. Box 19138, Arlington, TX, 76019-0138, USA.
E-mail address: ltang@uta.edu (L. Tang).

https://doi.org/10.1016/j.bioactmat.2020.06.019
Received 29 April 2020; Received in revised form 28 June 2020; Accepted 28 June 2020

alternative to avidin or streptavidin in avidin/biotin system-based pretargeting platforms [24]. Neutravidin is a deglycosylated derivative of avidin with an isoelectric point (pI) of ~6.3. The lack of the carbohydrate moieties and thus the nearly neutral pI reduces its nonspecific binding to surface of cells while preserving the high binding affinity with biotin [24].

Activated macrophages have been used as a biomarker for targeting inflammatory diseases [1,25–31]. Since inflammatory macrophages express a higher level of folate receptor (FR), FR has been extensively employed as the targeting site for inflammation diagnosis and treatment [32–34]. Ligand-conjugated polymeric micelles which target specific receptors on cells have been developed and applied for many disease diagnosis/treatment. Polymers are an attractive material for drug delivery because they are extraordinarily malleable and moldable for particles' sizes and shapes. Moreover, it can amplify encapsulation of outputs such as drugs or imaging agents [35], as well as they are biocompatible and biodegradable [3]. Based on the diverse modality of polymers, polymeric nanoparticles as nanomedicine had been broadly used not only for increasing drugs loading efficiency and tuning the releasing rate but also for prolonged circulation half-life of nanoplatform in circulatory system [25,36]. Activated macrophages have been shown to release inflammatory products, including IL-1, TNF-α, and reactive oxygen species [34] and the treatment of dexamethasone (Dex) has been shown to reduce macrophage activation and inflammatory responses [37–39]. Since systemic administration of Dex may lead to impaired wound repair and tissue regeneration [40], it is generally believed that targeted Dex delivery would produce more favorable healing outcome.

In the present work, we proposed a pretargeting "sandwich" platform to amplify anti-inflammation theragnosis via neutravidin-biotin system as schematically illustrated in Fig. 1. Specifically, an amphiphilic copolymer, poly(ethylene glycol-b-caprolactone) (PEG-PCL), was conjugated with either biotin or folate in order to prepare two different ligand-conjugated polymeric micelles. These biotinylated- and folate-conjugated optical imaging polymeric micelles (BFMC), pretargeted the activated macrophages at inflammatory sites via folate/FR interactions. After that, neutravidin proteins were delivered to bind with the BFMC via neutravidin/biotin interactions prior to Dex delivery by the second micelles, biotinylated polymeric drug carriers (BMC-Dex). Overall, our results support that the "sandwich" pretargeting platform can be a promising strategy not only for permit inflammatory diagnosis but also for enhance delivery of anti-inflammatory drugs to the inflamed tissues.

2. Experimental section

2.1. Materials

Amino-terminalized poly(ethylene glycol-b-caprolactone) (NH_2-PEG-PCL) (M_w:2200-b-7000) was purchased from Polymer Source Inc. (Dorval, Canada). D-Biotin, folate, avidin, neutravidin and Vybrant DiD cell labeling dye were obtained from Thermo Fisher Scientific (Waltham, MA). Dimethylformamide (DMF), dimethyl sulfoxide (DMSO), dimethyl sulfoxide-d_6 (DMSO-d_6), trimethylamine (TEA), tetrahydrofuran (THF), N-hydroxysuccinimide (NHS), N,N′-dicyclohexylcarbodiimide (DCC), folate binding protein (FBP), dexamethasone (Dex), fluorescein (FITC), lipopolysaccharide (LPS), and nile red (NR) were purchased from Sigma-Aldrich (St. Louis, MO). The murine macrophage RAW264.7 cells and murine NIH 3T3 cell line was obtained from the American Type Culture Collection (Rockville, MD, USA). Milli-Q grade deionized water was used through all experiments.

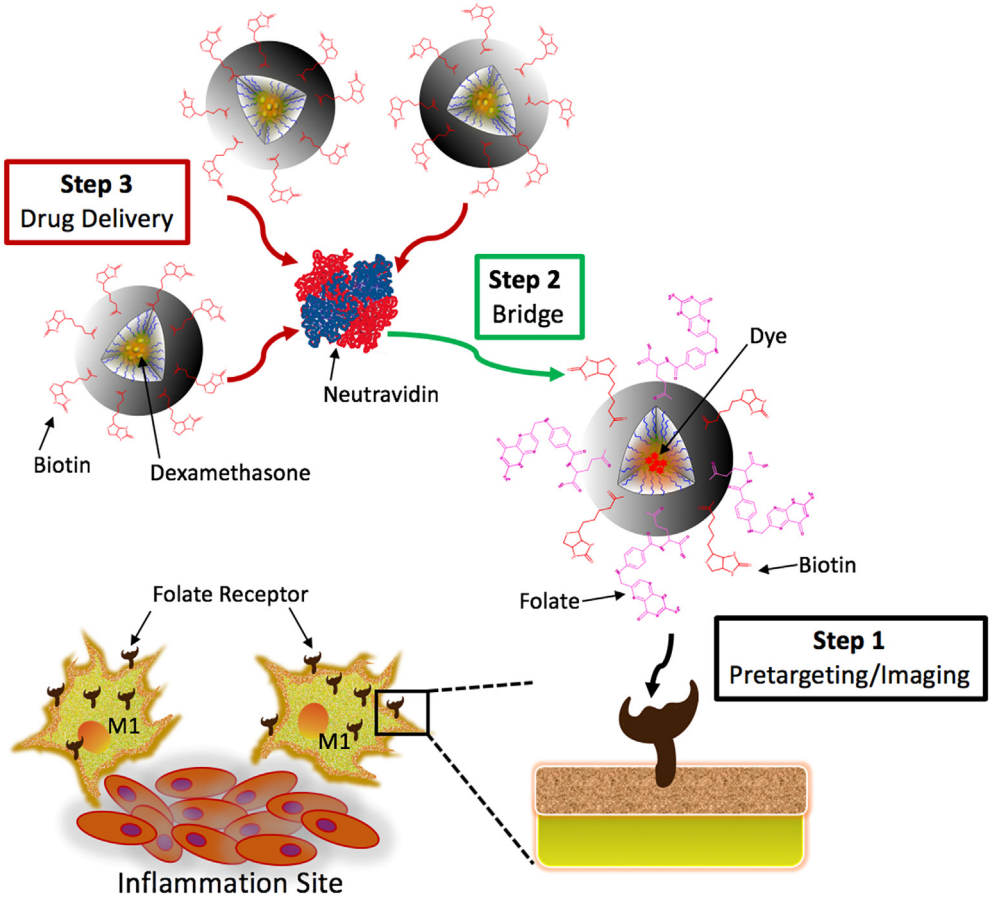

Fig. 1. Schematic illustration of the "sandwich" strategy for diagnosis/treatment for inflammatory diseases. The graphical presentation shows the amplified drug delivery to the inflammation site via neutravidin/biotin system combined with ligands-conjugated amphiphilic micelles.

2.2. Conjugation and characterization of ligand-conjugated amphiphilic polymers

To prepare folate-conjugated poly(ethylene glycol-b-caprolactone) (abbreviated as F-PEG-PCL), the carboxyl group of folate was initially activated according to a published paper [41]. Briefly, a 191.9 mg of folate was completely dissolved in 15.0 mL of DMF and stirred in the presence of a 100.0 mg of NHS and a 179.3 mg of DCC overnight at room temperature. After filtering out the byproduct, dicyclohexylurea (DCU), using a gravity filtration with filter papers, the activated folate was mixed with a 200.0 mg of NH_2-PEG-PCL dissolved in 2.5 mL DMSO followed by adding a 4.5 μL of TEA. The mixture was stirred overnight at room temperature, and then dialyzed against DI water for 48 h (dialysis tubing molecular weight cut-off, MWCO: 2 kD). The crude F-PEG-PCL conjugates were collected after the lyophilization. The dried powders were then re-dissolved in THF and the insoluble free folate was removed using filter papers. The filtrate was dialyzed against DI water again for 5 days to completely remove THF and unreactive free folate. The purified F-PEG-PCL was lyophilized to collect the final dried powders.

To prepare biotin-conjugated PEG-PCL (B-PEG-PCL), the carboxyl groups of biotin were activated as described above. Briefly, a 106.2 mg of biotin was dissolved in 5.0 mL of DMF completely, and then a 100.0 mg of NHS and a 179.3 mg of DCC were added. The activation reaction was preceded overnight at room temperature. Following the filtration of the precipitate with the filter papers, the activated biotin was mixed with 200.0 mg of NH_2-PEG-PCL dissolved in 2.5 mL of DMSO in the present of 4.5 μL of TEA. The mixture was then reacted overnight at room temperature as described above. Unconjugated biotin was removed by gravity filtration with ice-cold ethanol. The structures of the prepared conjugates, F-PEG-PCL as well as B-PEG-PCL, were determined by ^{1}H NMR. Briefly, the conjugated were prepared in DMSO-d_6 at the concentration of 10.0 mg/mL in a 5.0 mm NMR tube. NMR spectra were recorded on a Varian Gemini 2000 spectrometer working at 300 MHz for protons.

2.3. Preparation of fluorophore-loaded micelles

For *in vitro* studies, four different micelles were prepared, three micelles with FITC dye and one micelle with Nile Red dye. First, the FITC labeled- FMC and BMC as well as BFMC, a biotinylated-folate-conjugated (50:50) micelles were prepared followed by an emulsion/solvent evaporation method as described previously [42]. Briefly, 10.0 mg of either F-PEG-PCL or B-PEG-PCL along with 40.0 μg of FITC was dissolved in 2.0 ml of DMF, and then the mixture was added dropwise to 20.0 mL of DI water while sonicating at speed 5 (Ultrasonic processor XL, Misonix) for 1 min. After evaporating DMF under a gentle stirring for 14 h in a chemical hood, the prepared FMC-FITC (or BMC-FITC) was dialyzed against DI water for 16 h. The FMC-FITC (or BMC-FITC) solution was filtrated using 0.22 μm filters with syringes and then exchanged as well as concentrated with phosphate buffered saline (PBS) via ultrafiltration at 5,000 *g* (MWCO: 3 kD, Millipore, Massachusetts) for 15 min. All samples were kept at 1 mg/mL and 4 °C for later use. The BFMC micelles loaded with either FITC or Nile Red fluorophore (denoted as BFMC-FITC or BFMC-NR) were also prepared. Briefly, 5.0 mg of F-PEG-PCL and 5.0 mg of B-PEG-PCL, along with 40.0 μg of FITC (or Nile Red) were dissolved in 2.0 ml of DMF and the following progress was the same as described above.

The mean particle size and polydispersity index (PDI) of the prepared micelles were obtained by dynamic light scattering (DLS) using Malvern Zeta Sizer (Malvern Panalytical, Malvern, UK), and their morphologies were observed by high-resolution transmission electron microscopy, (HRTEM, H-9500, Hitachi, Japan). Additionally, Vybrant DiD-loaded micelles (BMC-DiD and FMC-DiD) were prepared for pre-targeting study *in vivo* (200.0 μg of DiD was loaded for 10.0 mg of polymer conjugates.)

2.4. In vitro targeting of the fluorophore-loaded micelles to folate binding protein

Targeting abilities of the prepared micelles (FMC-FITC, BMC-FITC, BFMC-FITC) to folate binding protein (FBP) were tested *in vitro*. FBP-coated Teflon disks (polytetrafluoroethylene, PFTE disks) were prepared as described before [43]. Briefly, PFTE disks with a diameter of 15 mm were rinsed with PBS solution and then dried in air. Then, 10.0 μL of FBP solution in PBS (0.24 μg/mL) was dropped on each of the PFTE disk and allowed to dry completely at 4.0 °C. To investigate the role of folate on micelle targeting, blocked FBPs with a 10.0 μl of folate solutions (concentration 3 and 30 μg/mL) were also prepared prior to the addition of the micelle's dispersions. Then, 10.0 μL of each prepared micelle (FMC-FITC, BMC-FITC and BFMC-FITC) were dropped on the top of the FBPs, and incubated for 30 min at room temperature. After a brief wash with PBS, fluorescent images of the targeted micelles to FBP were captured under a fluorescence microscope (Leica Microsystem GmbH, Wetzlar, Germany) combined with a Retiga-EXi CCD camera (QImaging, Surrey, BC, Canada) and intensities were processed via ImageJ software.

Second, a neutravidin-coated 96 well Nunc plate (Thermo Fisher Scientific, Grand Island, NY) was rinsed three times with a wash buffer containing 0.05% of Tween 20 in PBS. Then 200 μL of the prepared micelles (BMC-FITC, BFMC-FITC and FMC-FITC) were loaded into the wells. After incubation for 30 min at room temperature, the wells were washed triplicate with ash buffer to remove the unbound micelles prior to fluorescent intensity measurement. Furthermore, a set of competition experiments were carried out to investigate the biotin's role. For that, prior to the addition of the micelles, the free biotin with different concentrations (3 and 30 μg/mL) were incubated in the neutravidin-coated wells for 30 min. Fluorescent signals were recorded using a Tecan Infinite® 200 PRO microplate reader (Männedorf, Switzerland) with excitation at 470 nm and emission at 520 nm, respectively.

2.5. Evaluation of “sandwich” pretargeting platform In vitro

To confirm efficacy of a newly developed “sandwich” platform, targeting studies of the platform to inflammatory cells were performed *in vitro*. Mouse macrophage RAW264.7 cells (MΦs) were cultured in Dulbecco's modified Eagle's medium (DMEM) (Sigma-Aldrich, St. Louis, MO) supplemented with 10% fetal calf serum (Invitrogen, Carlsbad, CA) and 100 U/mL penicillin as well as 100 μg/mL streptomycin (Gibco, Waltham, MA) at 37 °C in a humidified 5% CO_2 incubator. MΦs were activated by culturing in the presence of 1 μg/mL of lipopolysaccharide (LPS, from *Escherichia coli*, Sigma, St Louis MO) overnight according to the previous publication [44].

First of all, for the “sandwich” pretargeting approach, the activated MΦs were first incubated with BFMC-NR (0.1 mg/mL) at 37 °C for 30 min (the first step-pretargeting), and then cultured for 30 min after addition of 0.1 mg/mL of neutravidin (the second step-bridging). The last incubation was in the presence of BMC-FITC (0.1 mg/mL) for another 30 min (the third step-drug delivery). Four different control groups were designed to investigate the roles of each step of the platform. The MΦs were washed after each step in PBS. Second, the “traditional” direct targeting method without applying the nanoplatform was also performed under the same condition. Briefly, the same amount of activated MΦs were incubated with FMC-FITC (0.1 mg/mL) for 30 min and washed on the same way. Fluorescence images of the targeted micelles to the MΦs were recorded using the fluorescent microscopy (Leica Microsystem GmbH, Wetzlar, Germany) combined with a Retiga-EXi CCD camera (QImaging, Surrey, BC, Canada). Additionally, suspended activated MΦs were also prepared for performing the same targeting study and quantifying the data using a Tecan Infinite® 200 PRO microplate reader (Männedorf, Switzerland). The suspended MΦs targeting study were performed with the same protocols above.

2.6. Preparation and characterization of an DEX-Loaded amphiphilic micelles

To investigate the therapeutic efficiency of the "sandwich" platform *in vivo*, an anti-inflammatory drug -Dex, Dex loaded-BMC and FMC micelles (denoted as BMC-Dex and FMC-Dex) were prepared according to a published method [45]. Briefly, 0.5 mg of Dex along with 10.0 mg of either F-PEG-PCL or B-PEG-PCL was dissolved in 2.0 ml of DMF completely. It was then dropped into a 20.0 ml of DI water while sonicating for 1 min. The mixture was then magnetically stirred for 14 h under a chemical hood to evaporate the organic solvent. The prepared micelle solutions were filtered using 0.22 μm filters with syringes. Finally, the purified FMC-Dex or BMC-Dex solutions were exchanged their media with PBS buffer via ultrafiltration (MWCO: 100 kD, Millipore, Massachusetts, USA) at 5,000 rpm for further use. The filtrates throughout the filters were all collected for measuring the actual drug loading efficiencies of the micelles. The amounts of free Dex in the filtrates were calculated by measuring absorbance at 242 nm using UV–Vis spectrophotometer (Model #8453, Agilent Technologies, Cary, North Carolina) so that the final amounts of entrapped Dex in FMC-Dex and BMC-Dex could be calculated. Encapsulation efficiency (EE %) (Equation (1).) and drug loading (DL %) (Equation (2).) were calculated using the formulas below.

$$Encapsulation\ Efficiency\ (\%) = \frac{Weight\ of\ Dex\ \ in\ micelles}{Weight\ of\ total\ feeding\ Dex} \times 100\% \quad (1)$$

$$Drug\ Loading\ (\%) = \frac{Weight\ of\ encapsulated\ Dex\ in\ micelles}{Weight\ of\ total\ micelles} \times 100\% \quad (2)$$

2.7. In vitro characterization of the release kinetic of Dex from amphiphilic micelles

A dialysis method was employed for assessing the drug release property of drug-loaded amphiphilic micelles as described earlier [46]. Briefly, 1 mL of each FMC-Dex or BMC-Dex in PBS as well as a 1 mL of free Dex in a PBS/DMSO (55:45 vol %) mixture were prepared in dialysis tubes (MWCO: 3.5–5 kD) separately. Those samples were incubated in 50 ml tubes with 5.0 mL of PBS (pH 7.4) at 37 °C as physiological media while shaking at 50 rpm in an incubator/shaker. 1 mL of Dex free micelles, FMC and BMC, were also prepared as control groups at the same condition. An aliquot 300 μL of the dialysate was collected from each sample at the set time points (10, 20 and 40 min, following 1, 2, 4, 6, 12, 24, 48, 72 and 80 h), and the same volume of pre-warmed PBS (pH 7.4) was refilled to maintain the total volume (5.0 mL) of dialysate. Absorbance of all the collected dialysates was measured at wavelength 242 nm using a UV–Vis spectrophotometer. The releasing rates of Dex were determined by measuring the absorbance of dialysates from each FMC-Dex or BMC-Dex as well as free Dex. The Absorbances of FMC or BMC was subtracted from the absorbance of FMC-Dex or BMC-Dex, respectively, to calculate amounts of released Dex only. The release experiment was carried out in triplicate.

2.8. In vivo therapeutic efficacy of the "sandwich" pretargeting platform

The therapeutic efficacy of the "sandwich" pretargeting platform to inflammation was evaluated using an implant-associated animal model as described in the previous publication [44]. All animal experiment protocols were approved by Animal Care and Use Committee of the UTA. In brief, 100.0 μL of the PLGA micron dispersions (60 mg/mL) were subcutaneously injected into the dorsal of Balb/C mouse (25 g body weight) obtained from The Jackson Laboratory (Bar Harbor, ME) to induce localized inflammatory responses. After 12 h of the implantations, a 1.0 mg of avidin was injected into each mouse in order to block the endogenous biotin in mouse 24 h prior to the treatments. The animals were then divided into four different groups; two control groups, either saline or free Dex injection group, and the "traditional" direct targeting approach as well as the "sandwich" pretargeting approach (Figure S1.). At step 1, 36 h after the implantation, the pretargeting agent, BFMC (concentration 1 mg/mL), was intraperitoneally administrated into mice for the "sandwich" group. At step 2, 4 h after the BFMC, neutravidin protein (concentration 1 mg/mL), served as an amplifying bridge, was administered intraperitoneally. Finally, at step 3, 4 h after the bridge, a mixture of BMC-Dex and BMC-DiD (the final concentration 1 mg/mL) were intravenously injected into mice. For the other three groups, a free DiD in saline, a free Dex along with DiD, or a mixture of FMC-Dex and FMC-DiD were injected, respectively. The enhancing effect of the new nanoplatform to target inflammatory site was monitored up to 7 days post-implantation using Kodak In-Vivo Imaging System FX Pro (Carestream Health Inc., New Haven, CT, USA). Three control groups were also performed with saline, free Dex and FMC-Dex injections, respectively. At the end of the study, implants and surrounding tissues were isolated and frozen sectioned. The tissue sections were subject to H&E and CD11b immunohistochemistry staining [44,47]. The histology images were taken utilizing a Leica fluorescence microscope (Leica Microsystem GmbH, Wetzlar, Germany) combined with a Retiga-EXi CCD camera (QImaging, Surrey, BC, Canada). Cell number was calibrated and quantified using ImageJ software.

2.9. Statistical analysis

All data was expressed as mean ± standard deviation. Significance was determined using either independent student t-test for the two independent groups or one-way analysis of variance (ANOVA) for the multi-groups. P values < 0.01 or 0.05 were considered statistically significant. At least triplicate tests were conducted for all statistical analysis.

3. Results

3.1. Characterization of the prepared folate- or biotin-conjugated copolymers

To prepare the polymeric micelles, we first conjugated folate or biotin on PEG-PCL copolymers separately using a carbodiimide coupling chemistry that was characterized using ^{1}H NMR. The characteristic peaks of PEG blocks (methane group at 3.65 ppm) and PCL blocks (methane group at 2.25 ppm) were first observed in free PEG-PCL copolymer. (Fig. 2A.). For folate-conjugated polymer, F-PEG-PCL, the ^{1}H NMR measurement showed the characteristic resonances of folate at 4.28, 4.51, 6.68, 7.66 and 8.64 ppm (Fig. 2B.) and the expanded peaks indicate the successful conjugation of folate into the PEG-PCL [41]. For biotin-conjugated polymer, B-PEG-PCL, biotin group was identified through two characteristic peaks which can be identified through the methane protons (a_1 and a_2) at 4.28 and 4.3 ppm (Fig. 2C.) [48]. The results support that biotin was successfully conjugated into PEG-PCL.

The conjugated polymers were then self-assembled into the micelles as a pretargeting/diagnostic agents or drug carriers. To investigate their ability to target folate receptors, fluorophores loaded folate-conjugated (FMC), biotin-conjugated (BMC) as well as both folate- and biotin-conjugated (BFMC) micelles were prepared by the self-assembly method. Dynamic light scattering (DLS) measurement showed that these prepared micelles were relatively monodispersed, and the average sizes of each micelle in diameters were 109.0 ± 48.4, 153.8 ± 87.8 and 156.1 ± 84.6 nm for BMC-FITC, BFMC-FITC and FMC-FITC, respectively (Fig. 3.). The polydispersity index (PDI) was 0.125, 0.326, and 0.294, and zeta potential of the polymeric micelles was −15.65 ± 3.64 mV, −12.86 ± 5.21 mV and −12.67 ± 3.89 mV for BMC-FITC, BFMC-FITC and FMC-FITC, respectively. These micelle's

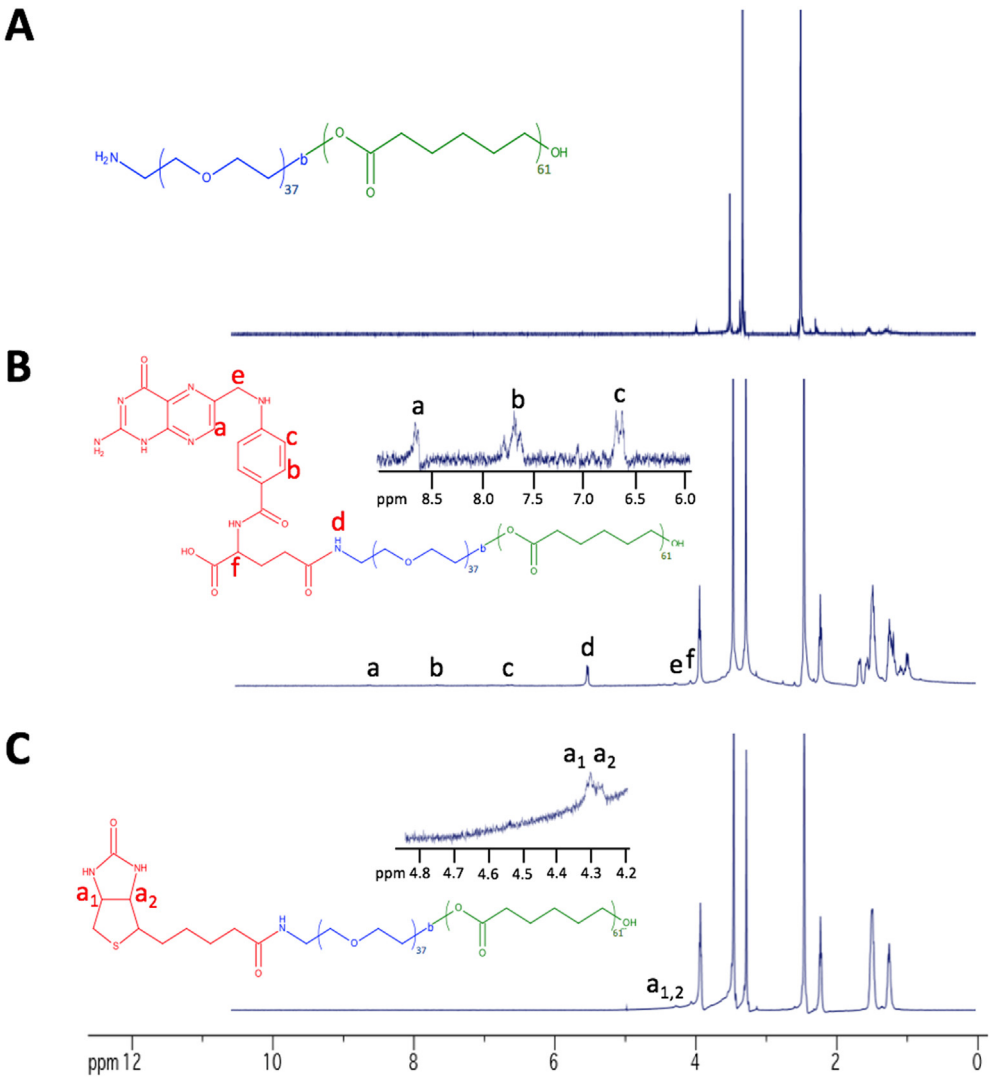

Fig. 2. ^{1}H NMR spectra of **A)** amino-terminalized poly(ethylene glycol-b-caprolactone) copolymers (NH_2-PEG2.2k-b-PCL7k), **B)** folate-conjugated copolymers (F-PEG-PCL) and **C)** biotin-conjugated copolymers (B-PEG-PCL) in DMSO-d_6. The expanded peaks "a" to "f" indicate the successful conjugations of the ligands on the block copolymers.

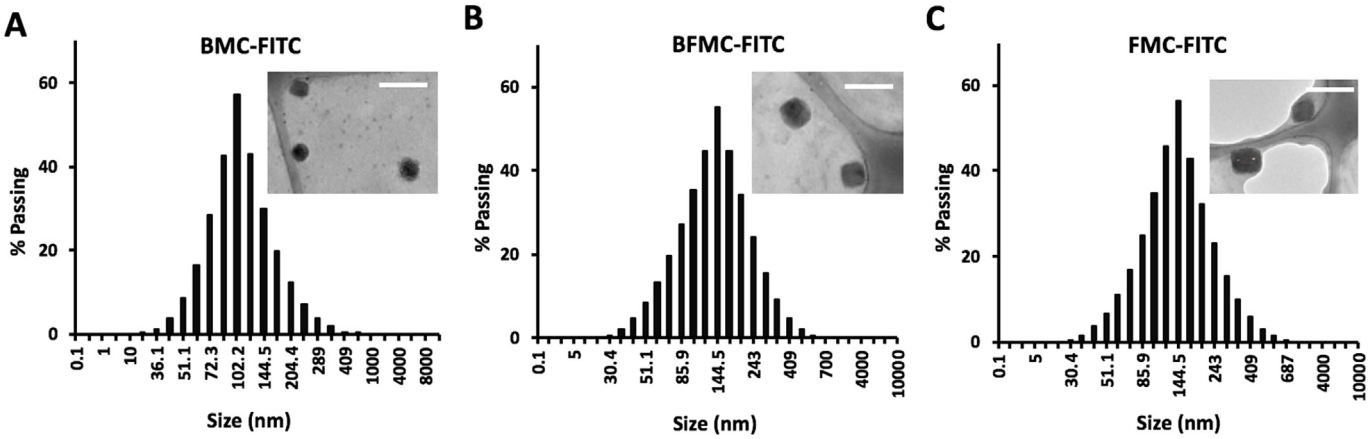

Fig. 3. Dynamic Light Scattering (DLS) measurements are demonstrating the size and polydispersities of each fluorescence dye-labeled amphiphilic micelle; **A)** BMC-FITC (109.0 ± 48.4 nm), **B)** BFMC-FITC (153.8 ± 87.8 nm) and **C)** FMC-FITC (156.1 ± 84.6 nm). Inserts: HRTEM images are illustrating that prepared micelles form spherical shapes. (Scale bar = 200 nm).

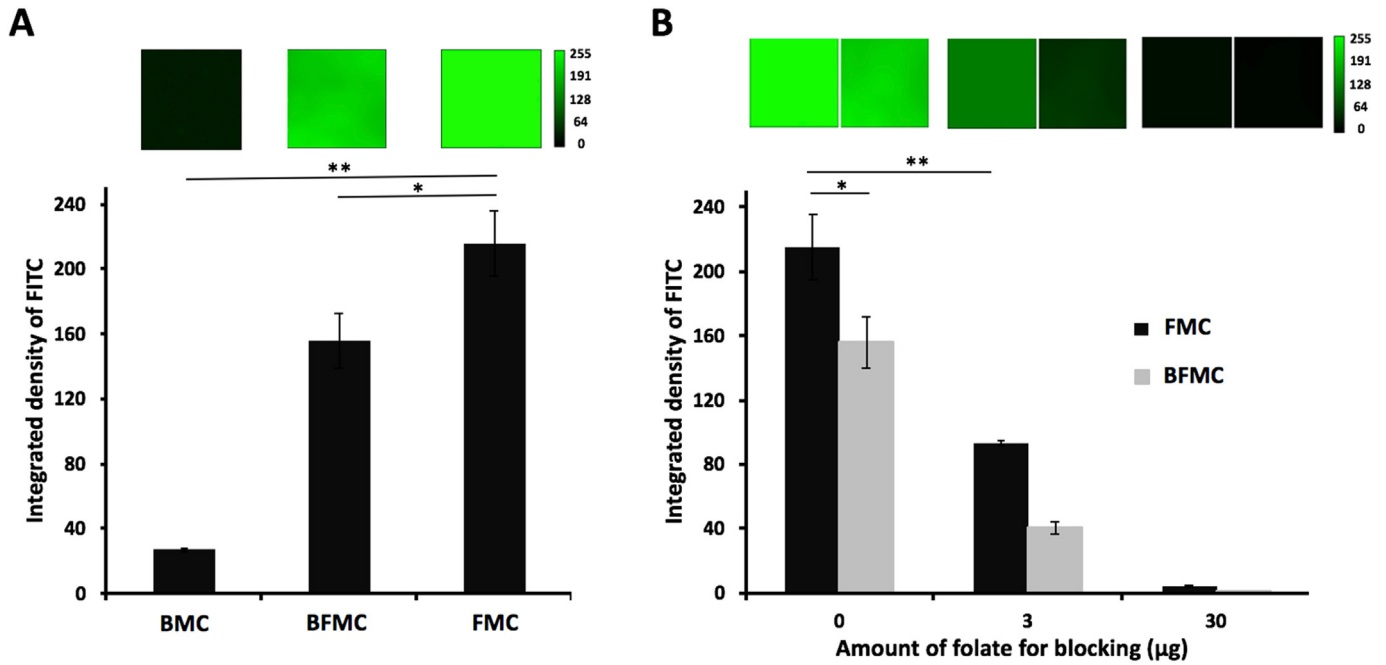

Fig. 4. *In vitro* binding affinity of amphiphilic micelles to folate binding protein (FBP) was determined. **A)** Folate conjugated micelles (FMC) and biotin-conjugated and folate conjugated micelles (BFMC) bind 8- and 6- fold more to folate binding protein (FBP) than biotinylated micelle (BMC), respectively. **B)** FBP was blocked with free folate prior to incubate with the micelles. Targeting affinity of FMC and BFMC to FBP was 2.3- and 3.9-fold reduced with 3.0 μg of folate blocking, respectively. This blocking study shows that free folate reduces the micelles accumulation on FBP in a dose dependent fashion. Data are mean ± standard deviation (n = 3, ANOVA, **p < 0.01 and *p < 0.05).

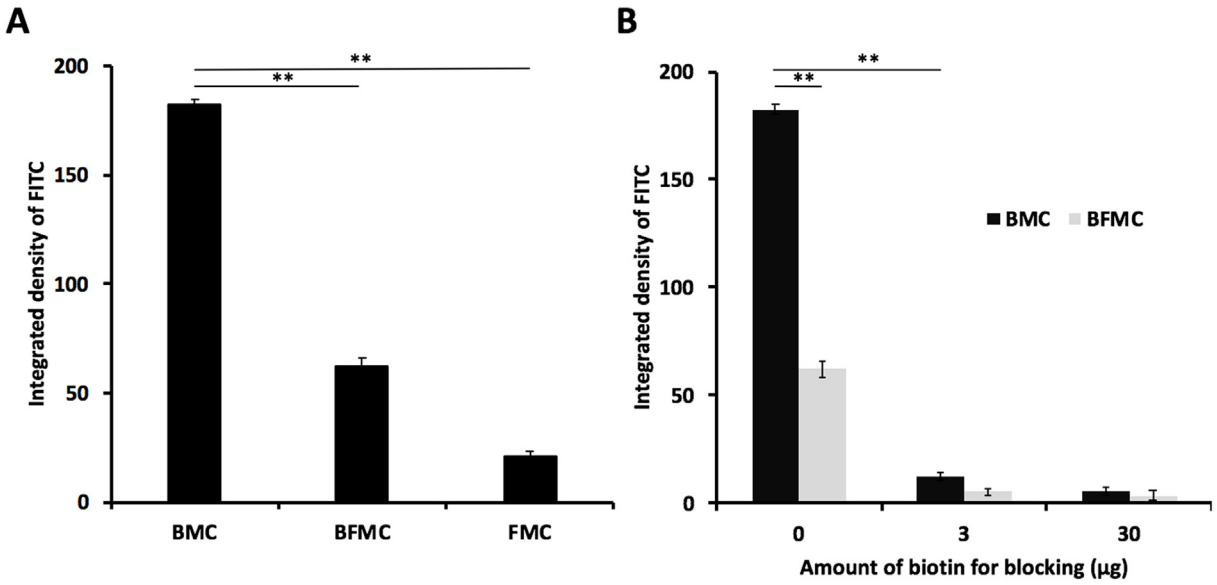

Fig. 5. *In vitro* study was carried out to determine the binding affinity of micelles to neutravidin coated wells. **A)** *In vitro* binding study between ligand-conjugated micelles and neutravidin concludes that biotin-conjugated micelle (BMC) and biotin- and folate-conjugated micelles (BFMC) binds 8.7- and 3- fold more to neutravidin than folate-conjugated micelle (FMC), respectively. **B)** Blocking study shows that free biotin reduces the micelle accumulation on neutravidin coated surface in a dose dependent fashion. Targeting affinity of BMC and BFMC to neutravidin was 14.5- and 11.3-fold reduced with 3.0 μg of biotin blocking, respectively. Data are mean ± standard deviation (n = 3, ANOVA, **p < 0.01).

colloidal stabilities in DI water were determined by monitoring the changes of particle sizes over time (up to 4 days). One can observe that BMC micelle has no significant changes, indicating that it is colloidally stable in water. On the other hand, the size of FMC micelles increases with the progression of time, causing probably by aggregation of the micelles. Further, the incorporation of B-PEG-PCL reduces aggregation of BFMC micelles (Figure S1). Further, the HRTEM images confirmed homogeneous and round-shaped morphology of the micelles in spite of a slight reduction of particle size due to dehydration during the process of sample preparation (Fig. 3., inserts). These prepared micelles were employed for next binding studies.

3.2. *In vitro binding study of the prepared micelles to folate binding protein*

The binding affinities of the prepared FITC-loaded BMC, BFMC and FMC micelles to folate binding protein (FBP) was determined after the

A

Steps	Cell only	Control 1	Control 2	Control 3	Sandwich platform
Pretargeting (BFMC-NR)	-	-	-	√	√
Bridge (Neutravidin)	-	√	-	-	√
Drug delivery (BMC-FITC)	-	√	√	√	√

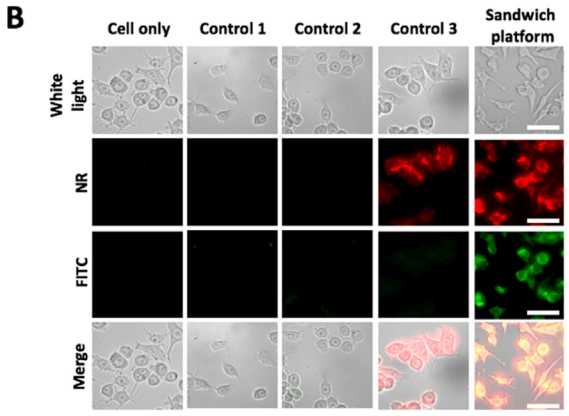

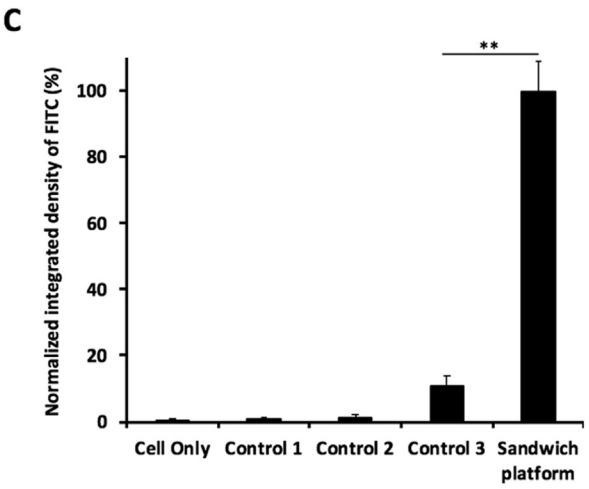

Fig. 6. *In vitro* macrophages targeting study of the new "sandwich" strategy. **A)** Activated macrophages were cultured and treated with four different groups and then the fluorescent images were captured under a fluorescent microscope. (Control 1: neutravidin + BMC-FITC (no step 1); Control 2: BMC-FITC (no step 1 and 2); Control 3: BFMC-NR + BMC-FITC (no step 2) and New Platform: the macrophages were treated sequentially with BFMC-NR (step 1), neutravidin (step 2) and BMC-FITC (step 3)) The fluorescent images show the strong signals of targeted BMC on macrophages via "sandwich" platform (Scale bar = 50 μm). **C)** The quantitative data shows the targeting ability of the new platform on suspended macrophages. Data are mean ± standard deviation (n = 3, ANOVA, **p < 0.01).

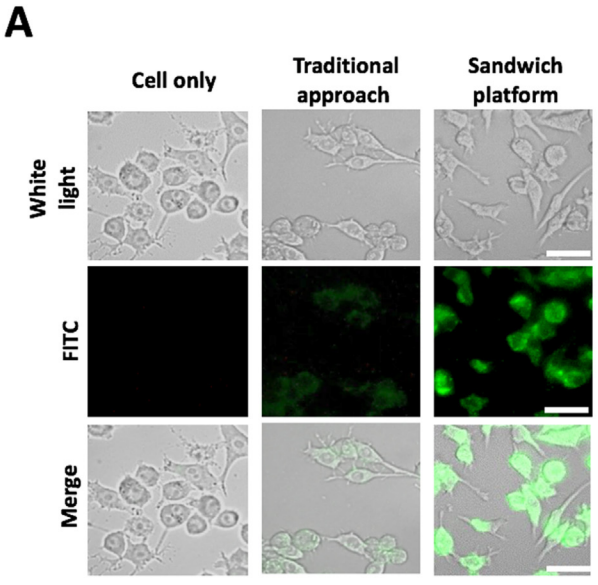

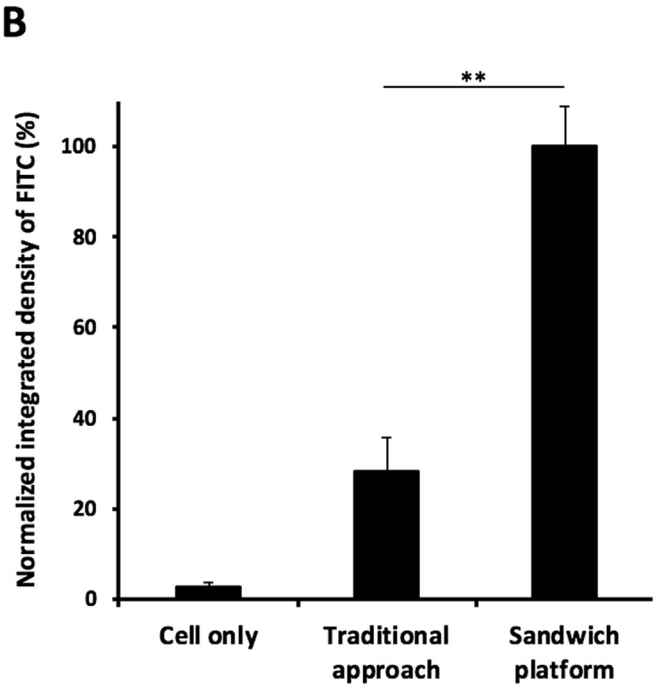

Fig. 7. The new "sandwich" pretargeting strategy emphasized 3.5 times more of the targeting efficacy to macrophages than the "traditional" direct targeting strategy. To show that, here two series of macrophage-targeting experiments were carried out. 1) FMC-FITC for the "traditional" approach and 2) BFMC-NR + neutravidin + BMC-FITC for the "sandwich" platform. **A)** Fluorescent microscope images show the amplified signals on macrophages with the second group (Scale bar = 40 μm). **B)** The quantitative data shows amplified BMC accumulation on suspended macrophages compared to the direct targeting approach. Data are mean ± standard deviation (n = 3, ANOVA, **p < 0.01).

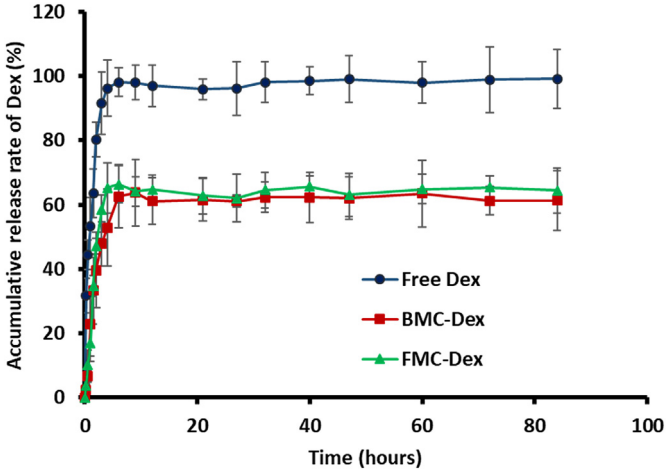

Fig. 8. Drug release properties of variously prepared amphiphilic micelles. *In vitro* release profiles of free Dex as well as Dex from the prepared three different micelles. Most of the free Dex (98%) was released out within the first 6 h but 66% and 62% of Dex only from FMC and BMC were released in 84 h, respectively.

30-minute incubation at room temperature. After incubated with BMC-FITC, we found no detectable fluorescent signal on FBP coated disks. On the other hand, after incubated with FMC-FITC or BFMC-FITC, bright green colors were observed on FBP-coated disks, indicating the strong interaction of those two micelles with FBP (Fig. 4A.). These results suggest that the BMC has little or no affinity to FBP-coated disks. Quantification analysis showed that compared to BMC, there were approximate 8- and 6-fold fluorescent intensities for FMC and BFMC, respectively. In addition, the incorporation of biotin group into BFMC only was observed to have a slight interference to binding ability to FBP (~27% reduction compared to FMC-FITC). To further confirm the role of folate ligands on the interaction of the micelles with FBP, a set of competition experiments was conducted in which the FBP-coated disks were incubated with the free folate prior to addition of the micelles. The results indicated that with increasing amount of free folate, the intensity of the fluorescent signal decreased (Fig. 4B.). These results support that the binding of the micelles to FBP is folate specific as well as folate concentration dependent.

3.3. In vitro binding study of the prepared micelles to neutravidin

Using neutravidin-coated well plates, we investigated the ability of the biotinylated micelle, BMC to interact with neutravidin by measurement of fluorescence intensities using a microplate reader [49]. As shown in Fig. 5A., there were fluorescent signals from wells treated with BMC-FITC and BFMC-FITC while there was a very weak signal associated with FMC-FITC-treated wells. Compared to FMC-FITC treatment, there were approximately 9-fold and 3-fold increases in fluorescent intensities with BMC-FITC and BFMC-FITC treatment, respectively. These results support a strong interaction of biotin presenting in micelles with neutravidin. To validate the binding specificity between biotinylated micelles and neutravidin, competition experiments were conducted in which different concentrations of free biotin were added into the culture media prior to the incubation with micelles (Fig. 5B.). It showed that fluorescent intensities decreased gradually as the amount of free biotin increased. These results support the indispensable role of the biotin in binding of the micelles to neutravidin. In addition, we find the prepared micelles are cell compatible, since the micelles (FMC/BFMC/BMC) have no significantly toxicity to 3T3 fibroblasts up to 1 mg/ml (Figure S2).

3.4. In vitro assessment of the "sandwich" platform to target activated macrophages

To further evaluate the effect of the new nanoplatform to target macrophages (MΦs), two different fluorophores-loaded micelles were used; BFMC-NR for the pretargeting step and the BMC-FITC for the following amplifying step. In Fig. 6A. & 6.B., the pretargeting platform significantly increased the accumulation of BMC on activated MΦs (the strong FITC signal). On the other hand, one can observe that, without either BFMC-NR treatment (Control 1) or BFMC-NR and neutravidin (Control 2) treatment, the accumulation of BMC on the activated MΦs was significantly reduced (very weak FITC signals). Meanwhile, the strong NR signals without the bridge, neutravidin, (Control 3) showed that BFMC was able to bind to the activated MΦs via interactions between folate of BFMC and folate receptor on MΦs. However, the lack of neutravidin treatment prevented BMC from accumulating on macrophages. The quantified data (in Fig. 6C.) performed with prepared

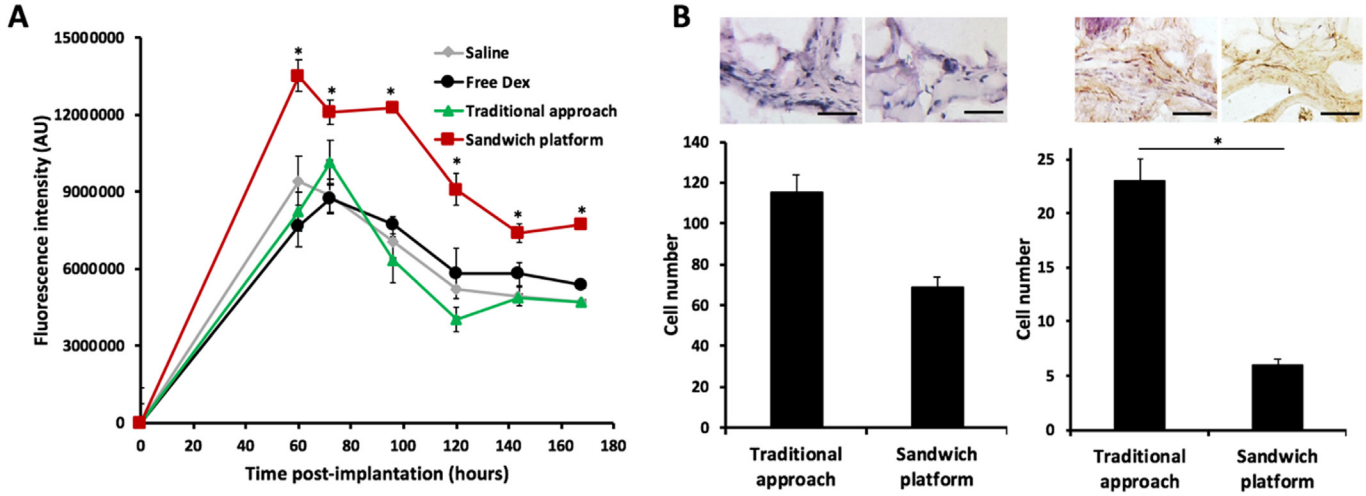

Fig. 9. Theranostics efficiency of the "sandwich" platform *in vivo* was assessed by measuring signals of targeted imaging agents as well as counting CD11b + inflammatory cells at the inflammation sites. **A)** The fluorescent intensities at the implantation sites were recorded at different time points up to 7 days post-implantation. The "sandwich" pretargeting platform amplified 1.5-fold of drug delivery rate than the direct delivery. Data are mean ± standard deviation (n = 3, ANOVA, *p < 0.05). **B)** Densities of cells (H&E staining) and CD11b + inflammatory cells at the inflamed sites were quantified histologically at 7 days post-implantation. The data shows 56.5% reduction of the number of CD11b + inflammatory cells in implantation sites. Data are mean ± standard deviation (n = 3, ANOVA, *p < 0.05) and the scale bar indicates 50 μm.

suspended MΦs confirmed that the effective bio-recognition between folate and its receptor on activated MΦs, as well as the biotin and neutravidin interaction, played an important role on achievement and enhancement of the micelle homing to MΦs (the enhanced FITC fluorescent signals).

The amplifying signal of the pretargeting platform (sandwich approach) was then compared to a direct targeting method (traditional approach) (Fig. 7A.). Fluorescent signals could still be observed with the direct targeting approach. However, once the same activated macrophages were treated with the sandwich approach, the fluorescent signal was significantly amplified. The quantitative analysis (Fig. 7B.) also showed an approximate 3.5-fold amplifying in fluorescent intensity compared to the direct targeting approach. These *in vitro* MΦs targeting studies had confirmed that the new pretargeting platform allowed more micelles to accumulate on the activated MΦs than the direct targeting approach via folate/folate receptor and biotin/neutravidin interactions. Therefore, the strategy may be used to improve the efficiency of drug delivery to inflammatory sites.

3.5. In vitro dex release study of the amphiphilic micelles

Dexamethasone was loaded into BMC and FMC micelles. Encapsulation efficiency (EE %) was calculated to 61 and 79% while drug loading (DL%) was estimated to 1.8 and 1.2% for BMC and FMC, respectively. *In vitro* release study showed that free Dex was released really fast with up to 98% release over the first 6 h (Fig. 8). On the other hand, approximately 66 and 62% of Dex were released from FMC and MMC micelles in 84 h, respectively. Our results are similar to those of the previous study [45], suggesting that the Dex loaded micelles can slow down the release of Dex at a physiological environment.

3.6. In vivo evaluation of efficacy of the new nanoplatform on treating inflammation

Finally, the efficiency of the pretargeting platform to amplify drug delivery and to reduce inflammatory responses was assessed using a murine subcutaneous inflammatory response model. For that, subcutaneous and localized inflammatory responses were induced by implantation of poly-lactic acid particles. After implantation for 36 h which is the optimal time to trigger the accumulation of inflammatory cells at the implantation site, animals were treated with either the traditional or the sandwich approaches by following a time line as depicted in Figure S3. By analyzing the fluorescent intensities at the implant site (Figure S4), we found that, as anticipated, pretargeting platform delivered the highest number of the drug carriers, BMC, to the inflamed tissue sites up to 7 days (Fig. 9A.). It is estimated that the number of Dex-loaded BMC delivered by the pretargeting approach is ~1.5 folds of those by the traditional approach. The enhanced delivery of Dex-loaded micelles was confirmed by histological analyses. Finally, histology analyses on the extent of inflammatory responses at the implant sites also revealed that the pretargeting approach has led to signification reduction (56.5%) of CD11b + inflammatory cells by compared with the traditional approach (Fig. 9B.). The overall results support the overall design criteria of the new pretargeting approach, as it significantly improves targeted drug delivery and amplifies the anti-inflammatory efficacy of Dex-loaded micelles.

4. Discussion and conclusions

Although avidin/biotin system has been widely investigated as pretargeting platforms for tumor theragnosis [49,50], little effort has been made to explore the potential of using the same strategy to treat inflammatory diseases. To find the answer, a novel pretargeting nanoplatform via neutravidin/biotin system was designed to target activated macrophages infiltrated in inflammatory diseases for theranostic purposes. Neutravidin is used here because the absence of the carbohydrate moieties makes it slightly acidic (pI: ~6.3), enabling prevention of its nonspecific binding to cell surfaces and proteins [19]. The temporarily separated three steps strategy was designed with two different surface-engineered micelles and a protein as a bridge between them. Briefly, Step 1: folate- and biotin-conjugated polymeric micelles were designed to target folate receptor which are highly expressed on activated MΦs. Step 2: neutravidin protein is employed as a bridge for amplifying accumulation of drug-loaded cargos. Step 3: biotinylated micelles, which caged an anti-inflammatory drug, enhanced accumulation at the inflammatory sites by attaching to neutravidin protein.

To test the hypothesis, PEG-PCL copolymer were employed to prepare micelles due to its controlled biodegradability and high biocompatibility [45]. Folate- or biotin-conjugated polymers as well as polymeric micelles were successfully prepared. The following *in vitro and in vivo* studies confirmed that the new nanoplatform is a promising anti-inflammatory drug delivery system for targeting activated macrophages and amplifying anti-inflammatory responses. It is well documented that the activated macrophage is a biomarker of inflammation, and folate receptors are upregulated on surfaces of these activated macrophages [34,51]. Activated macrophages (up-regulating folate receptor) experiments show that compared to the traditional direct targeting method, the pretargeting platform can significantly improve the micelles homing to the activated macrophages. Since occurrence of the inflammatory lesion triggers macrophage infiltration and activation, the activated macrophages can be used as a target for delivery of imaging reporter/drug. Our drug delivery strategy may be further explored for the treatment of the other diseases. For example, via replacing folate ligand with amino-terminal peptide encompassing amino acids 2–26 (Ac2-26), the delivery system may be used to deliver imaging agent or drug to the vascular injured/inflammatory sites by targeting the exposed Collagen IV.

In short, the neutravidin/biotin integrated pretargeting “sandwich” platform was successfully prepared. Both *in vitro* and *in vivo* testing confirmed that the pretargeting platform can effectively detect inflamed tissue via fluorescent imaging first, and then amplify the delivery of anti-inflammatory drug (Dex) at an inflammatory site. The pretargeting nanoplatform may be further developed so that it becomes spatiotemporal control platform for intractable diseases at right moment, right place and right dose for personalized inflammatory diseases treatment. Finally, the pretargeting platform can easily be modified for treating different inflammatory diseases or other illnesses.

CRediT authorship contribution statement

Min Kyung Khang: Data curation, Formal analysis, Writing - original draft. **Jun Zhou:** Conceptualization, Writing - review & editing. **Cynthia M. Co:** Data curation, Formal analysis. **Shuxin Li:** Data curation, Formal analysis, Writing - review & editing. **Liping Tang:** Conceptualization, Funding acquisition, Supervision, Project administration, Writing - review & editing.

Declaration of competing interest

Authors claim no conflicts of interest.

Acknowledgements

We thank YiHui Huang and Samira Izuagbe for assistance in conducting the animal work and cell cytotoxicity test. This work was partially supported by a grant from Wilson Charitable Foundation Trust (WCFT). The authors acknowledge the financial support from the National Heart, Lung and Blood Institute with the award number NIH T32 HL134613. The content is solely the responsibility of the authors and does not necessarily represent the official views of the NIH and WCFT.

Appendix A. Supplementary data

Supplementary data to this article can be found online at https://doi.org/10.1016/j.bioactmat.2020.06.019.

References

[1] S.K. Patel, J.M. Janjic, Macrophage targeted theranostics as personalized nanomedicine strategies for inflammatory diseases, Theranostics 5 (2) (2015) 150–172, https://doi.org/10.7150/thno.9476.

[2] J.H. Ryu, S. Lee, S. Son, S.H. Kim, J.F. Leary, K. Choi, I.C. Kwon, Theranostic nanoparticles for future personalized medicine, J. Contr. Release 190 (2014) 477–484, https://doi.org/10.1016/j.jconrel.2014.04.027.

[3] B.T. Luk, L. Zhang, Current advances in polymer-based nanotheranostics for cancer treatment and diagnosis, ACS Appl. Mater. Interfaces 6 (24) (2014) 21859–21873, https://doi.org/10.1021/am5036225.

[4] E.K. Lim, T. Kim, S. Paik, S. Haam, Y.M. Huh, K. Lee, Nanomaterials for theranostics: recent advances and future challenges, Chem. Rev. 115 (1) (2015) 327–394, https://doi.org/10.1021/cr300213b.

[5] J.V. Jokerst, S.S. Gambhir, Molecular imaging with theranostic nanoparticles, Acc. Chem. Res. 44 (10) (2011) 1050–1060, https://doi.org/10.1021/ar200106e.

[6] R. Kumar, W.S. Shin, K. Sunwoo, W.Y. Kim, S. Koo, S. Bhuniya, J.S. Kim, Small conjugate-based theranostic agents: an encouraging approach for cancer therapy, Chem. Soc. Rev. 44 (2015) 6670–6683, https://doi.org/10.1039/c5cs00224a.

[7] M. Patra, K. Zarschler, H.J. Pietzsch, H. Stephan, G. Gasser, New insights into the pretargeting approach to image and treat tumours, Chem. Soc. Rev. 45 (23) (2016) 6415–6431, https://doi.org/10.1039/c5cs00784d.

[8] S.J. Knox, M.L. Goris, M. Tempero, P.L. Weiden, L. Gentner, H. Breitz, G.P. Adams, D. Axworthy, S. Gaffigan, K. Bryan, D.R. Fisher, D. Colcher, I.D. Horak, L.M. Weiner, Phase II trial of yttrium-90-DOTA-biotin pretargeted by NR-LU-10 antibody/streptavidin in patients with metastatic colon cancer, Clin. Canc. Res. 6 (2) (2000) 406–414.

[9] R.M. Sharkey, D.M. Goldenberg, Cancer radioimmunotherapy, Immunotherapy 3 (3) (2011) 349–370, https://doi.org/10.2217/imt.10.114.

[10] F.C.J. van de Watering, M. Rijpkema, M. Robillard, W.J.G. Oyen, O.C. Boerman, Pretargeted imaging and radioimmunotherapy of cancer using antibodies and bioorthogonal chemistry, Front. Med. 1 (44) (2014) 1–11, https://doi.org/10.3389/fmed.2014.00044.

[11] M. Altai, R. Membreno, B. Cook, V. Tolmachev, B.M. Zeglis, Pretargeted imaging and therapy, J. Nucl. Med. 58 (10) (2017) 1553–1559, https://doi.org/10.2967/jnumed.117.189944.

[12] G. Liu, D.J. Hnatowich, A semiempirical model of tumor pretargeting, Bioconjugate Chem. 19 (11) (2008) 2095–2104, https://doi.org/10.1021/bc8002748.

[13] C.R. Divgi, Status of radiolabeled monoclonal antibodies for diagnosis and therapy of cancer, Oncology 10 (6) (1996) 939–953.

[14] R.B. Walter, O.W. Press, J.M. Pagel, Pretargeted radioimmunotherapy for hematologic and other malignancies, Cancer Biother. Radiopharm. 25 (2) (2010) 125–142, https://doi.org/10.1089/cbr.2010.0759.

[15] L. Tienken, N. Drude, I. Schau, O.H. Winz, A. Temme, E. Weinhold, F.M. Mottaghy, A. Morgenroth, Evaluation of a pretargeting strategy for molecular imaging of the prostate stem cell antigen with a single chain antibody, Sci. Rep. 8 (2018) 1–9, https://doi.org/10.1038/s41598-018-22179-y.

[16] J.C. Knight, B. Cornelissen, Bioorthogonal chemistry: implications for pretargeted nuclear (PET/SPECT) imaging and therapy, Am. J. Nucl. Med. Mol. Imag. 4 (2014) 96–113 http://www.ncbi.nlm.nih.gov/pubmed/24753979%0Ahttp://www.pubmedcentral.nih.gov/articlerender.fcgi?artid=PMC3992206.

[17] H.P. Lesch, M.U. Kaikkonen, J.T. Pikkarainen, S. Ylä-Herttuala, Avidin-biotin technology in targeted therapy, Expert Opin, Drug Deliv. 7 (5) (2010) 551–564, https://doi.org/10.1517/17425241003677749.

[18] H. Zhou, J. Liu, J.J. Xu, S.S. Zhang, H.Y. Chen, Optical nano-biosensing interface: via nucleic acid amplification strategy: construction and application, Chem. Soc. Rev. 47 (6) (2018) 1996–2019, https://doi.org/10.1039/c7cs00573c.

[19] A. Jain, K. Cheng, The principles and applications of avidin-based nanoparticles in drug delivery and diagnosis, J. Contr. Release 245 (2017) 27–40, https://doi.org/10.1016/j.jconrel.2016.11.016.

[20] S.M. Larson, J.A. Carrasquillo, N.K.V. Cheung, O.W. Press, Radioimmunotherapy of human tumours, Nat. Rev. Canc. 15 (6) (2015) 347–360, https://doi.org/10.1038/nrc3925.

[21] S.C. Meyer, T. Gaj, I. Ghosh, Highly selective cyclic peptide ligands for neutravidin and avidin identified by phage display, Chem. Biol. Drug Des. 68 (1) (2006) 3–10, https://doi.org/10.1111/j.1747-0285.2006.00401.x.

[22] R. Alon, E.A. Bayer, M. Wilchek, Streptavidin contains an RYD sequence which mimics the RGD receptor domain of fibronectin, Biochem. Biophys. Res. Commun. 170 (3) (1990) 1236–1241, https://doi.org/10.1016/0006-291X(90)90526-S.

[23] R.M. Sharkey, H. Karacay, T.M. Cardillo, C.H. Chang, W.J. McBride, E.A. Rossi, I.D. Horak, D.M. Goldenberg, Improving the delivery of radionuclides for imaging and therapy of cancer using pretargeting methods, Clin. Canc. Res. 11 (2005) 7109–7122, https://doi.org/10.1158/1078-0432.CCR-1004-0009.

[24] H.W. Wen, T.R. Decory, W. Borejsza-Wysocki, R.A. Durst, Investigation of NeutrAvidin-tagged liposomal nanovesicles as universal detection reagents for bioanalytical assays, Talanta 68 (4) (2006) 1264–1272, https://doi.org/10.1016/j.talanta.2005.07.032.

[25] W. Xu, P. Ling, T. Zhang, Polymeric micelles, a promising drug delivery system to enhance bioavailability of poorly water-soluble drugs, J. Drug Deliv. 2013 (2013) 340315, https://doi.org/10.1155/2013/340315.

[26] R. Kojima, D. Aubel, M. Fussenegger, Novel theranostic agents for next-generation personalized medicine: small molecules, nanoparticles, and engineered mammalian cells, Curr. Opin. Chem. Biol. 28 (2015) 29–38, https://doi.org/10.1016/j.cbpa.2015.05.021.

[27] B.R. Smith, S.S. Gambhir, Nanomaterials for in vivo imaging, Chem. Rev. 117 (3) (2017) 901–986, https://doi.org/10.1021/acs.chemrev.6b00073.

[28] P.S. Low, W.A. Henne, D.D. Doorneweerd, Discovery and development of folic-acid-based receptor targeting for imaging and therapy of cancer and inflammatory diseases, Acc. Chem. Res. 41 (1) (2008) 120–129, https://doi.org/10.1021/ar7000815.

[29] J.B. Kim, K. Park, J. Ryu, J.J. Lee, M.W. Lee, H.S. Cho, H.S. Nam, O.K. Park, J.W. Song, T.S. Kim, D.J. Oh, D.G. Gweon, W.Y. Oh, H. Yoo, J.W. Kim, Intravascular optical imaging of high-risk plaques in vivo by targeting macrophage mannose receptors, Sci. Rep. 6 (2016) 22608, https://doi.org/10.1038/srep22608.

[30] J.M. Tarkin, F.R. Joshi, J.H.F. Rudd, PET imaging of inflammation in atherosclerosis, Nat. Rev. Cardiol. 11 (8) (2014) 443–457, https://doi.org/10.1038/nrcardio.2014.80.

[31] G. Pawelec, D. Goldeck, E. Derhovanessian, Inflammation, ageing and chronic disease, Curr. Opin. Immunol. 29 (2014) 23–28, https://doi.org/10.1016/j.coi.2014.03.007.

[32] M. Nahrendorf, H. Zhang, S. Hembrador, P. Panizzi, D.E. Sosnovik, E. Aikawa, P. Libby, F.K. Swirski, R. Weissleder, Nanoparticle PET-CT imaging of macrophages in inflammatory atherosclerosis, Circulation 117 (3) (2008) 379–387, https://doi.org/10.1161/CIRCULATIONAHA.107.741181.

[33] R. Weissleder, M. Nahrendorf, M.J. Pittet, Imaging macrophages with nanoparticles, Nat. Mater. 13 (2014) 125–138, https://doi.org/10.1038/nmat3780.

[34] W. Han, R. Zaynagetdinov, F.E. Yull, V.V. Polosukhin, L.A. Gleaves, H. Tanjore, L.R. Young, T.E. Peterson, H.C. Manning, L.S. Prince, T.S. Blackwell, Molecular imaging of folate receptor β-positive macrophages during acute lung inflammation, Am. J. Respir. Cell Mol. Biol. 53 (2015) 50–59, https://doi.org/10.1165/rcmb.2014-0289OC.

[35] C.M. Paulos, M.J. Turk, G.J. Breur, P.S. Low, Folate receptor-mediated targeting of therapeutic and imaging agents to activated macrophages in rheumatoid arthritis, Adv. Drug Deliv. Rev. 56 (2004) 1205–1217, https://doi.org/10.1016/j.addr.2004.01.012.

[36] S. Zhang, J. Ermann, M.D. Succi, A. Zhou, M.J. Hamilton, B. Cao, J.R. Korzenik, J.N. Glickman, P.K. Vemula, L.H. Glimcher, G. Traverso, R. Langer, J.M. Karp, An inflammation-targeting hydrogel for local drug delivery in inflammatory bowel disease, Sci. Transl. Med. 7 (300) (2015), https://doi.org/10.1126/scitranslmed.aaa5657 300ra128.

[37] N.H. Waldron, C.A. Jones, T.J. Gan, T.K. Allen, A.S. Habib, Impact of perioperative dexamethasone on postoperative analgesia and side-effects: systematic review and meta-analysis, Br. J. Anaesth. 110 (2) (2013) 191–200, https://doi.org/10.1093/bja/aes431.

[38] J.W. Pollard, Trophic macrophages in development and disease, Nat. Rev. Immunol. 9 (4) (2009) 259–270, https://doi.org/10.1038/nri2528.

[39] Y.T. Tsai, J. Zhou, H. Weng, J. Shen, L. Tang, W.J. Hu, Real-time noninvasive monitoring of in vivo inflammatory responses using a ph ratiometric fluorescence imaging probe, Adv. Healthc. Mater. 3 (2) (2014) 221–229, https://doi.org/10.1002/adhm.201200365.

[40] C.Y. Ko, L. Wu, A.M. Nair, Y.T. Tsai, V.K. Lin, L. Tang, The use of chemokine-releasing tissue engineering scaffolds in a model of inflammatory response-mediated melanoma cancer metastasis, Biomaterials 33 (3) (2012) 876–885, https://doi.org/10.1016/j.biomaterials.2011.10.002.

[41] X. Yang, W. Deng, L. Fu, E. Blanco, J. Gao, D. Quan, X. Shuai, Folate-functionalized polymeric micelles for tumor targeted delivery of a potent multidrug-resistance modulator FG020326, J. Biomed. Mater. Res. 86 (1) (2008) 48–60, https://doi.org/10.1002/jbm.a.31537.

[42] H. Gao, G. Hu, Q. Zhang, S. Zhang, X. Jiang, Q. He, Pretreatment with chemotherapeutics for enhanced nanoparticles accumulation in tumor: the potential role of G2 cycle retention effect, Sci. Rep. 4 (2014) 4492, https://doi.org/10.1038/srep04492.

[43] N. Minoura, S. Aiba, Y. Gotoh, M. Tsukada, Y. Imai, Attachment and growth of cultured fibroblast cells on silk protein matrices, J. Biomed. Mater. Res. 29 (10) (1995) 1215–1221, https://doi.org/10.1002/jbm.820291008.

[44] J. Zhou, Y.T. Tsai, H. Weng, D.W. Baker, L. Tang, Real time monitoring of biomaterial-mediated inflammatory responses via macrophage-targeting NIR nanoprobes, Biomaterials 32 (2011) 9383–9390, https://doi.org/10.1016/j.biomaterials.2011.08.064.

[45] Q. Wang, J. Jiang, W. Chen, H. Jiang, Z. Zhang, X. Sun, Targeted delivery of low-dose dexamethasone using PCL-PEG micelles for effective treatment of rheumatoid arthritis, J. Contr. Release 230 (2016) 64–72, https://doi.org/10.1016/j.jconrel.2016.03.035.

[46] M. Bartneck, F.M. Peters, K.T. Warzecha, M. Bienert, L. van Bloois, C. Trautwein, T. Lammers, F. Tacke, Liposomal encapsulation of dexamethasone modulates cytotoxicity, inflammatory cytokine response, and migratory properties of primary human macrophages, Nanomed. Nanotechnol. Biol. Med. 10 (2014) 1209–1220, https://doi.org/10.1016/j.nano.2014.02.011.

[47] C.Y. Ko, L.X. Wu, A.M. Nair, Y.T. Tsai, V.K. Lin, L.P. Tang, The use of chemokine-releasing tissue engineering scaffolds in a model of inflammatory response-mediated melanoma cancer metastasis, Biomaterials 33 (2012) 876–885, https://doi.org/10.1016/j.biomaterials.2011.10.002.

[48] S.V.K. Rompicharla, P. Kumari, H. Bhatt, B. Ghosh, S. Biswas, Biotin functionalized PEGylated poly(amidoamine) dendrimer conjugate for active targeting of paclitaxel in cancer, Int. J. Pharm. 557 (2019) 329–341, https://doi.org/10.1016/J.

IJPHARM.2018.12.069.
[49] T. Maldiney, M.U. Kaikkonen, J. Seguin, Q. Le Masne De Chermont, M. Bessodes, K.J. Airenne, S. Ylä-Herttuala, D. Scherman, C. Richard, In vitro targeting of avidin-expressing glioma cells with biotinylated persistent luminescence nanoparticles, Bioconjugate Chem. 23 (3) (2012) 472–478, https://doi.org/10.1021/bc200510z.
[50] R. Kalluri, Basement membranes: structure, assembly and role in tumour angiogenesis, Nat. Rev. Canc. 3 (6) (2003) 422–433, https://doi.org/10.1038/nrc1094.
[51] J.M. Chan, L. Zhang, R. Tong, D. Ghosh, W. Gao, G. Liao, K.P. Yuet, D. Gray, J.-W. Rhee, J. Cheng, G. Golomb, P. Libby, R. Langer, O.C. Farokhzad, Spatiotemporal controlled delivery of nanoparticles to injured vasculature, Proc. Natl. Acad. Sci. U. S. A 107 (5) (2010) 2213–2218, https://doi.org/10.1073/pnas.0914585107.